The Journal of Chemical Physics ARTICLE scitation.org/journal/jcp

Calibration of a lattice model for high-molecular-weight block copolymer melts

Cite as: J. Chem. Phys. 150, 204906 (2019); doi: 10.1063/1.5094144
Submitted: 27 February 2019 • Accepted: 6 May 2019 •
Published Online: 30 May 2019

View Online Export Citation CrossMark

J. D. Willis,[1] T. M. Beardsley,[1] and M. W. Matsen[1,2,3,a)]

AFFILIATIONS

[1] Department of Physics, University of Waterloo, Waterloo, Ontario N2L 3G1, Canada
[2] Department of Chemical Engineering, University of Waterloo, Waterloo, Ontario N2L 3G1, Canada
[3] Waterloo Institute for Nanotechnology, University of Waterloo, Waterloo, Ontario N2L 3G1, Canada

[a)] **Electronic mail:** mwmatsen@uwaterloo.ca

ABSTRACT

The Morse calibration is applied to a lattice model designed for efficient simulations of two-component polymer melts of high molecular weight. The model allows multiple occupancy per site, which results in high invariant polymerization indices, and interactions are limited to monomers within the same site, which enhances the computational speed. The calibration maps the interaction parameter of the lattice model, α, onto the Flory-Huggins χ parameter of the standard Gaussian-chain model, by matching the disordered-state structure function, $S(k)$, of symmetric diblock copolymers to renormalized one-loop predictions. The quantitative accuracy of the calibration is tested by comparing the order-disorder transition of symmetric diblock copolymer melts to the universal prediction obtained from previous simulations. The model is then used to confirm the universality of fluctuation corrections to the critical point of symmetric binary homopolymer blends.

Published under license by AIP Publishing. https://doi.org/10.1063/1.5094144

I. INTRODUCTION

Block copolymer phase behavior is understood to be universal in the high-molecular-weight limit.[1] This implies that all models reduce to the standard Gaussian-chain model (GCM),[2] which underpins most block copolymer calculations, including self-consistent field theory (SCFT),[3] the random-phase approximation (RPA),[4] and strong-stretching theory (SST).[5] The standard GCM is a minimal model that contains only the essential features of the system and as such involves the least number of parameters possible. Its mean-field behavior for monodisperse AB diblock copolymer melts is controlled by just three quantities: the composition f, the ratio of segment lengths a_A/a_B, and the product χN, where N is the total polymerization and χ is the Flory-Huggins interaction parameter.[6] Fluctuation corrections to the mean-field behavior are then controlled by one additional parameter, the invariant polymerization index $\bar{N} = a^6\rho_0^2 N$, where $a = [fa_A^2 + (1-f)a_B^2]^{1/2}$ is the average segment length and ρ_0 is the segment density.[7] Note that we follow the usual practice of defining all segments to have a common volume of ρ_0^{-1}.

To exploit the universality, one needs to map the parameters of a given model onto those of the standard GCM. The mapping of molecular compositions (e.g., f) is trivial, given their straightforward definition in terms of volume fraction. Segment lengths are also clearly defined by the requirement that the radius of gyration of linear polymers in an athermal melt reduces to $R_g = a(N/6)^{1/2}$ in the limit of large N. The nontrivial part of the mapping is between the χ parameter of the GCM and a corresponding parameter of the particle-based model, α, specifying the strength of its A-B interactions in units of k_BT. The relationship needs to be determined by matching the behavior of the given model to some prediction of the GCM. In principle, it could be any quantity for any block copolymer system, but it is best to choose the most accurate prediction possible that permits fits to relatively large values of α. With this in mind, Morse and co-workers[8] chose the renormalized one-loop (ROL) prediction for the disordered-state structure

Published under license by AIP Publishing

function, $S(q)$, of symmetric diblock copolymer melts (i.e., $f = 0.5$ and $a_A/a_B = 1$).[9,10]

Glaser *et al.*[11] demonstrated the universality by comparing the order-disorder transition (ODT) of symmetric diblock copolymer melts from five distinct models. Four were off-lattice bead-spring models and one was a simple lattice model. When expressed in terms of the calibrated parameters, the ODTs from all five models collapsed onto a universal curve,

$$(\chi N)_{\mathrm{ODT}} = 10.495 + 41.0\bar{N}^{-1/3} + 123.0\bar{N}^{-0.56}. \quad (1)$$

The equivalence between models has since been illustrated for a number of other quantities of symmetric diblocks[12] and for the disordered-state structure function of asymmetric diblocks.[13] Furthermore, the universality between simulation and experiment has also been demonstrated.[14]

Given that all models, both lattice and off-lattice, produce equivalent results, it makes sense to use the most computationally efficient. In this regard, lattice models offer significant advantages by restricting the N monomers of each polymer to the sites of an artificial lattice, allowing simulations to cope with far larger polymerizations. However, the quantity that really matters is the invariant polymerization index, $\bar{N} = a^6\rho_0^2 N$. Hence, it is advantageous to use models with a large density, ρ_0. Typical lattice models[15–19] allow only one monomer per site leading to relatively low densities, whereas off-lattice models with soft interactions[8] can result in much larger densities, ρ_0. Nevertheless, lattice models can also handle large densities, provided they allow more monomers per site.[20]

Here, we introduce a multiple-occupancy lattice model similar to the one proposed by Wang,[20] which permits large monomer densities while retaining the computational efficiency of a lattice. This facilitates simulations at invariant polymerizations, $10^3 \lesssim \bar{N} \lesssim 10^4$, typical of high-molecular-weight polymers.[21] After applying the Morse calibration, the model is used to test the universality of multicomponent melts. In the first instance, we compare the ODTs of symmetric diblock copolymer melts to the universal curve in Eq. (1). Next, the critical points of symmetric binary homopolymer blends are compared with the prediction,

$$(\chi N)_c = 2 + c\bar{N}^{-1/2} + O(\bar{N}^{-1}), \quad (2)$$

where the coefficient c is believed to be universal. It was initially estimated by ROL to be $c \approx 3.4$,[23] but this prediction is inaccurate because ROL does not treat critical fluctuations properly. A recent lattice simulation found a much smaller $c \approx 1.5$,[24] but the universality of this value remains to be corroborated.

II. MONTE CARLO SIMULATIONS

Our simulations all involve melts of n linear polymers, each consisting of N monomers labeled sequentially by $s = 1, 2, \ldots, N$. In the case of symmetric diblock copolymers, the monomers at $s \le N/2$ are designated as A-type, while the remaining ones are denoted as B-type (N is chosen to be even). For the homopolymer blends, n_A of the molecules are A-type, while the remaining $n_B = n - n_A$ are B-type. The polymer chains are all placed on a lattice of M sites, with a maximum of Z monomers per site and with bonded monomers occupying nearest-neighbor sites. Both systems use a Hamiltonian,

$$\frac{H}{k_BT} = \alpha n_{AB}, \quad (3)$$

that is proportional to the total number of AB contacts,

$$n_{AB} = \sum_{j=1}^{M} n_{A,j} n_{B,j}, \quad (4)$$

where $n_{\gamma,j}$ is the number of γ-type monomers at site j.

The lattice coordinates are given by $\mathbf{r}_j = d(h, k, l)$, where h, k, and l are integers ranging from 1 to L. By only permitting even values of $h + k + l$, we obtain an fcc lattice with $M = L^3/2$ sites and a bond length of $b = \sqrt{2}d$. The application of periodic boundary conditions requires L to be even. In order to allow room for the polymers to move, 20% of the sites contain a single vacancy (i.e., an occupancy of $Z - 1$ monomers), which results in an average density of

$$\rho_0 \equiv nN/V = (Z - 0.2)\sqrt{2}/b^3, \quad (5)$$

where $nN = (Z - 0.2)M$ is the total number of monomers and $V = (Ld)^3 = Mb^3/\sqrt{2}$ is the volume of the system.

The equilibrium behavior of this model is investigated by Metropolis Monte Carlo simulations, where the Monte Carlo steps (MCS) randomly select among several different types of trial moves. The first is a slithering snake (or reptation) move. It is performed by randomly choosing one of the $2n$ chain ends and one of its 12 nearest-neighbor sites to move to. The remaining monomers of the chain are shifted one site along its contour. The move is immediately rejected if it causes a violation in the allowed number of monomers at a site, and otherwise, its acceptance is determined by the Metropolis criterion. The second is a crankshaft move, where one of the $n(N - 2)$ nonend monomers is selected at random and moved while keeping its two bonded neighbors fixed. If the initial site already has a vacancy or there are no potential sites with a vacancy, then the move is rejected. Otherwise, one of the potential sites is selected at random and the Metropolis criterion is applied. The third is a double-bridging move that swaps equal portions of the chain between two polymers.[22] This move is performed by selecting a random site and looking for pairs of nonend monomers corresponding to the same index, s. If there are none, then the move is rejected. Otherwise, we choose a pair with s closest to the middle of the chain and swap the bonds between the s and $s + 1$ monomers. For diblock copolymer melts, our algorithm also permits a polymer to perform a complete chain reversal (i.e., a head-to-tail flip). For homopolymer blends, we include a move whereby molecules can change their type from A to B or vice versa, which results in a semigrand canonical ensemble.[24]

III. MORSE CALIBRATION

We now calibrate the lattice model for $Z = 5$. The calibration begins with simulations of athermal melts (i.e., $\alpha = 0$) of different polymerization, N. In each case, the simulation box is chosen sufficiently large to accommodate $n \approx 5000$ molecules. In order to fill the lattice to the desired density, the polymers are placed on the

Published under license by AIP Publishing

lattice in extended conformations. Given this highly artificial state, we perform a long equilibration of 10^6 MCS per monomer before collecting statistics.

In order to determine the invariant polymerization index, $\bar{N}$, we need the statistical segment length, a. This is obtained by evaluating the radius of gyration squared,

$$R_g^2 = \left\langle \frac{1}{N}\sum_{s=1}^{N} |\mathbf{r}_s - \mathbf{R}_{cm}|^2 \right\rangle, \tag{6}$$

where $\mathbf{r}_s$ is the position of the sth monomer and

$$\mathbf{R}_{cm} = \frac{1}{N}\sum_{s=1}^{N} \mathbf{r}_s \tag{7}$$

is the center of mass. The angle brackets denote an average, which is evaluated from simulations of approximately 10^6 MCS per monomer, where all n molecules are sampled once every 10^3 MCS per monomer. The results are plotted in Fig. 1(a) for different polymerizations, N, and fit to[23]

$$\frac{6R_g^2}{b^2 N} = a^2\left[1 - \frac{1.42}{a^3\rho_0 N^{1/2}} + \frac{\gamma}{N}\right], \tag{8}$$

where a and γ are fitting parameters. The fit gives a segment length of $a = 1.0447b$, which, in turn, implies

$$\bar{N} = a^6\rho_0^2 N = 59.9\,N. \tag{9}$$

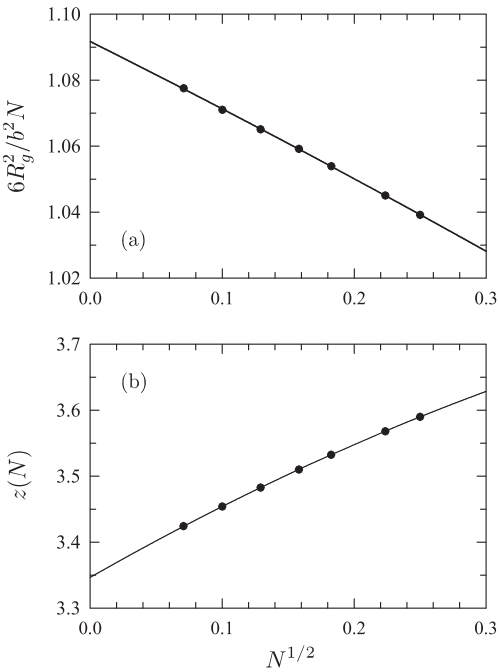

FIG. 1. (a) Radius of gyration squared, R_g^2, and (b) number of intermolecular contacts per monomer, $z(N)$, plotted in terms of polymerization, N, for $Z = 5$. Simulation results are denoted by symbols, and fits to Eqs. (8) and (10) are shown with solid curves. The statistical uncertainties are smaller than the symbol size.

In the limit of weak interactions, the Flory-Huggins χ parameter becomes linear in α. To match the simulations to SCFT in the large-N limit, the proportionality constant has to be set to $z_\infty = \lim_{N\to\infty} z(N)$, where $z(N)$ is the average number of intermolecular contacts per monomer in an athermal melt of polymerization N. Therefore, while collecting statistics for R_g^2, we also count the number of intermolecular contacts per monomer. The results are plotted in Fig. 1(b) for different polymerizations, N, and fit to[25]

$$z(N) = z_\infty\left[1 + \frac{(6/\pi)^{3/2}}{a^3\rho_0 N^{1/2}} + \frac{\delta}{N}\right], \tag{10}$$

where z_∞ and δ are fitting parameters. The fit gives $z_\infty = 3.346$, from which we obtain the linear approximation, $\chi \approx z_\infty\alpha$, for weak interactions.

To determine the Flory-Huggins χ parameter for strong interactions, we evaluate the structure function of symmetric diblock copolymer melts over a series of α values spanning the disordered phase. The structure function is obtained from the ensemble average

$$S(\mathbf{q}) = \frac{1}{4V}\left\langle \left| \sum_{j=1}^{M} m_j \exp(i\mathbf{q}\cdot\mathbf{r}_j) \right|^2 \right\rangle, \tag{11}$$

where $m_j = (n_{A,j} - n_{B,j})/(Z - 0.2)$. Because our simulation box is finite, the wavevector is limited to the discrete values $\mathbf{q} = 2\pi(h, k, l)/Ld$, where h, k, and l are integers. After each step in α, we first equilibrate the system for 10^5 MCS per monomer and then collect statistics over 10^6 MCS per monomer, sampling once every 10^3 MCS per monomer. Since the disordered state is isotropic, we also average over wavevectors of equal magnitude, $q \equiv |\mathbf{q}|$. Figure 2 shows $S(q)$ for diblock copolymers containing $N = 30$ monomers. The peaks of the structure function, $S(q^*)$, are obtained from fits to the RPA structure function,[4] shown by solid curves.

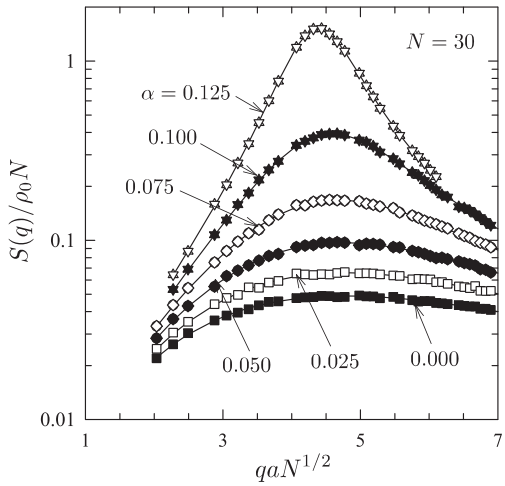

FIG. 2. Structure function, $S(q)$, for diblock copolymers of polymerization $N = 30$ plotted for different interaction parameters, α. Symbols denote simulation results, and solid curves are fits used to extract the peak height, $S(q^*)$.

Published under license by AIP Publishing

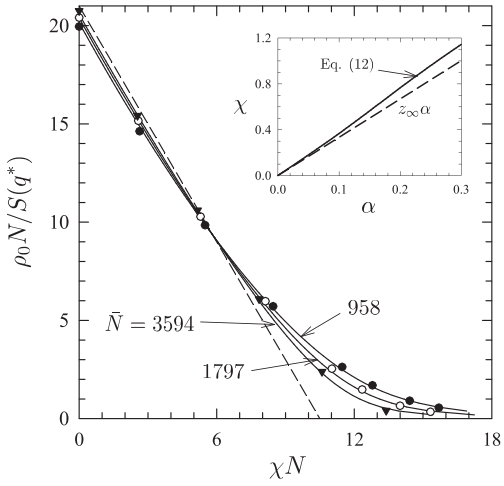

FIG. 3. Inverse peak height of the structure function, $S^{-1}(q^*)$, plotted in terms of the effective χ parameter for different invariant polymerization indices, $\bar{N}$. Symbols denote simulation results, solid curves are ROL predictions, and the dashed line is the RPA prediction. The inset shows the nonlinear $\chi = z_\infty \alpha + c_1\alpha^2 + c_2\alpha^3$ with a solid curve and the linear approximation $\chi \approx z_\infty \alpha$ with a dashed line.

The $S(q^*)$ for diblock copolymers of N = 16, 20, 30, 40, and 60 are fit to ROL theory, assuming the nonlinear relationship

$$\chi = z_\infty \alpha + c_1 \alpha^2 + c_2 \alpha^3. \tag{12}$$

The fit gives $c_1 = 4.16$ and $c_2 = -8.66$. Figure 3 demonstrates the quality of the fit for three of the polymerizations; for clarity, the N = 20 and 40 results have been omitted. The inset compares the resulting α-dependence of χ with the linear approximation $\chi \approx z_\infty \alpha$.

IV. ODT OF DIBLOCK COPOLYMER MELTS

To confirm that our model adheres to the universality hypothesis, we compare the ODT for symmetric diblock copolymers to Eq. (1). This is done by simulating multiple replicas of the system at a series of α values spanning the expected ODT, all initialized with disordered configurations. The replicas are run in parallel, each following the usual MC algorithm for approximately 10^6 MCS per monomer. The ODT is identified by evaluating the average number of AB contacts, $\langle n_{AB} \rangle$, over the last 10^4 MCS per monomer. Past studies[11,26] have demonstrated that $\langle n_{AB} \rangle$ changes abruptly at the transition.

During the simulations, highly metastable defects often nucleate impeding the formation of a well-ordered morphology, particularly when α is large. To help remedy this problem, we implement parallel tempering,[28,29] whereby a swap between a random pair of replicas at neighboring α values is attempted every 10^3 MCS per monomer (see Ref. 26 for more details). In this way, defect structures are shifted to lower segregation, which allows them to anneal out more easily. By the end of our simulations, all the ordered replicas exhibited defectfree lamellae. Even with parallel tempering, the metastability of the disordered phase may cause an overestimation of $(\alpha N)_{ODT}$. Therefore, we run a second set of parallel-tempering simulations, starting from ordered lamellar configurations obtained from the first runs. The second runs will tend to underestimate $(\alpha N)_{ODT}$, thus allowing us to bracket the true equilibrium ODT.

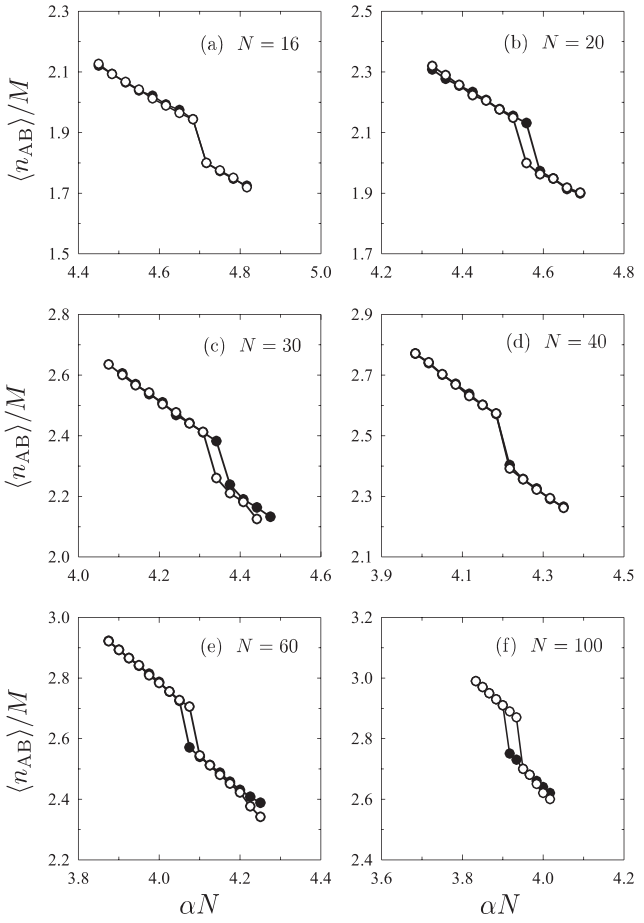

FIG. 4. Average number of AB contacts, $\langle n_{AB} \rangle$, from parallel-tempering simulations of diblock copolymers with polymerizations of (a) N = 16, (b) N = 20, (c) N = 30, (d) N = 40, (e) N = 60, and (f) N = 100. Solid and open symbols denote simulations initialized with ordered and disordered configurations, respectively.

TABLE I. Order-disorder transition, $(\alpha N)_{ODT}$, for diblock copolymer melts of different polymerization, N, obtained from Fig. 4. Our uncertainty in the $(\alpha N)_{ODT}$ estimates is about 1%. Also listed are the system sizes, L, the lamellar orientations, (hkl), and the lamellar periods, D.

N	$(\alpha N)_{ODT}$	L	(hkl)	$D/aN^{1/2}$
16	4.70	30	(311)	1.53
20	4.56	30	(300)	1.51
30	4.34	40	(311)	1.49
40	4.20	50	(320)	1.48
60	4.08	60	(320)	1.45
100	3.93	80	(321)	1.45

Published under license by AIP Publishing

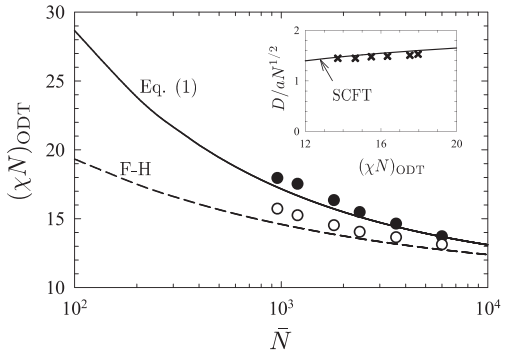

FIG. 5. ODTs from Table I plotted in terms of the nonlinear $\chi = z_\infty\alpha + c_1\alpha^2 + c_2\alpha^3$ (solid circles) and the linear approximation $\chi \approx z_\infty\alpha$ (open circles); the symbol size corresponds to our 1% uncertainty. The solid curve denotes the universal prediction in Eq. (1),[11] while the dashed curve shows the Fredrickson-Helfand prediction.[7] The inset compares the lamellar periods, D, listed in Table I (crosses) with the SCFT prediction (solid curve).[6]

Figure 4 plots $\langle n_{\rm AB}\rangle$ from the parallel-tempering runs for a series of polymerizations. For each N, the runs from order and disorder produce very similar curves, indicating that nonequilibrium effects are relatively minor. The narrow metastability intervals pin down the ODTs to a relative accuracy of about 1%. The ODTs are listed in Table I, along with the size of the simulation box L, the orientation of the lamellar phase (hkl), and the lamellar period $D = Ld/\sqrt{h^2+k^2+l^2}$.

Figure 5 plots the ODTs from Table I in terms of χN and $\bar{N} = 59.9N$, to allow comparison with the universal curve [Eq. (1)]. The agreement illustrates that the calibration is successful for experimentally relevant molecular weights. The inset compares the period, D, of the lamellar phase at $(\chi N)_{\rm ODT}$ with the SCFT prediction for the same value of χN.[6] The reasonable agreement is consistent with a previous conclusion that SCFT provides an accurate treatment of ordered phases.[12]

V. CRITICAL POINT OF POLYMER BLENDS

Our next application of the model examines the critical points, α_c, of symmetric homopolymer blends. Because the correlation length diverges as $\alpha \to \alpha_c$, the finite size of the simulation box will affect the results no matter how large L is. Therefore, we apply the finite-scaling approach of Binder,[27] which involves calculating the cumulant

$$U_L = 1 - \frac{\langle \bar{m}^4\rangle}{3\langle \bar{m}^2\rangle^2}, \tag{13}$$

for a series of system sizes, L, where $\bar{m} = (n_A - n_B)/n$. The critical point corresponds to the value of α for which U_L is independent of L.

In order to reduce the computational effort, we employ Monte Carlo reweighting[28,29] to calculate the α-dependence of the moments, $\langle \bar{m}^k\rangle$. This involves running one long simulation of around 10^6 MCS per monomer at an α_0 close to the transition and storing the values of $\bar{m}$ and the number of AB contacts, n_{AB}, every 40 MCS per monomer. The ensemble average of $\bar{m}^k$ at α is then given by

$$\langle \bar{m}^k\rangle = \frac{\sum_i \bar{m}_i^k \exp(n_{AB,i}(\alpha_0 - \alpha))}{\sum_i \exp(n_{AB,i}(\alpha_0 - \alpha))}. \tag{14}$$

Naturally, the reweighing will become inaccurate if α differs too much from α_0. Fortunately, reweighting works particularly well near a critical point due to the broad distribution of configurations resulting from the critical fluctuations. To be absolutely safe, we repeat the simulation if our initial choice of α_0 differs from α_c by more than 0.5%.

Figure 6 plots the cumulants for different polymerizations, demonstrating the expected behavior where the curves cross at a fixed point. This identifies the critical points, α_c, listed in Table II. The estimated uncertainty in these values is 0.1%, based on the spread among the crossing points for different pairs of system sizes,

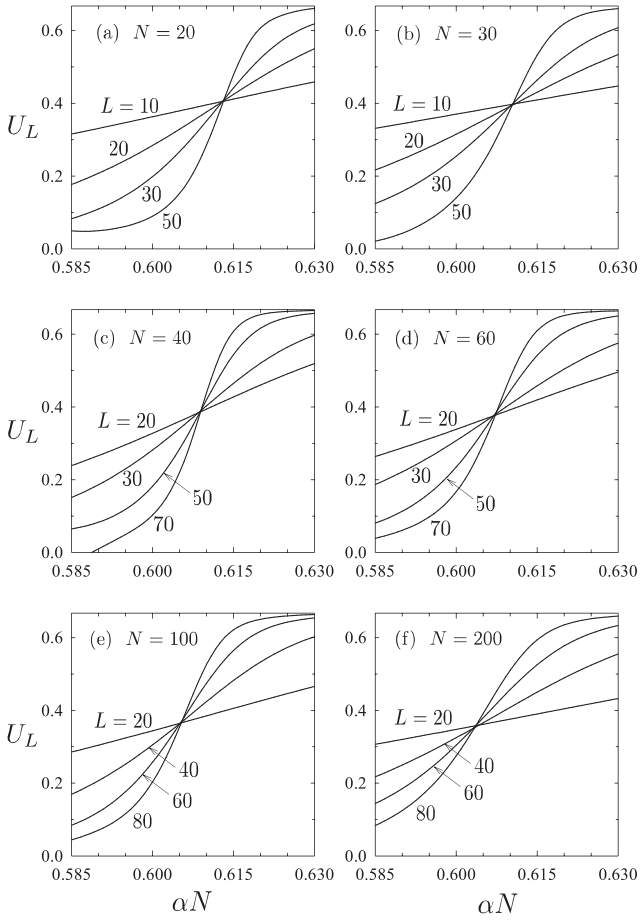

FIG. 6. Binder cumulants, U_L, for a series of system sizes, L, calculated for homopolymer blends with polymerizations of (a) $N = 20$, (b) $N = 30$, (c) $N = 40$, (d) $N = 60$, (e) $N = 100$, and (f) $N = 200$. The crossing points provide accurate estimates of the critical transition, α_c.

Published under license by AIP Publishing

TABLE II. Critical points, $(\alpha N)_c$, for homopolymer blends of different polymerizations, N, obtained from Fig. 6. Our uncertainty in the $(\alpha N)_c$ estimates is about 0.1%.

N	$(\alpha N)_c$
20	0.6129
30	0.6103
40	0.6088
60	0.6070
100	0.6051
200	0.6034

L. Figure 7 replots the cumulants with the temperature axis scaled by $L^{1/\nu}$, where $\nu = 0.629\,97$ is the critical exponent of the correlation length for the 3D-Ising universality class. The near perfect collapse of the curves confirms that the finite-size scaling is working properly.

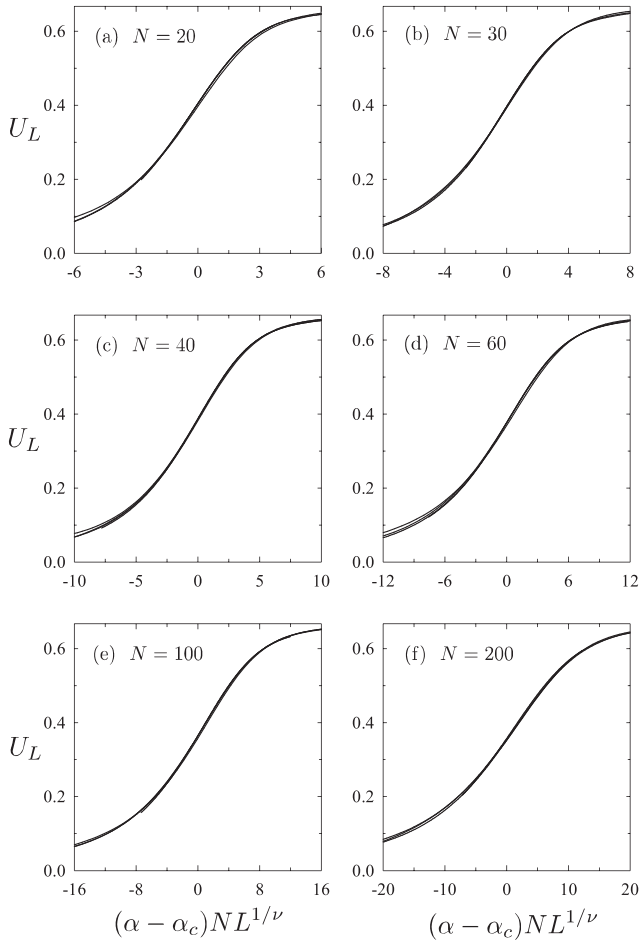

FIG. 7. Binder cumulants from Fig. 6 for homopolymer blends with polymerizations of (a) $N = 20$, (b) $N = 30$, (c) $N = 40$, (d) $N = 60$, (e) $N = 100$, and (f) $N = 200$ replotted with the horizontal axis scaled by $L^{1/\nu}$, where $\nu = 0.629\,97$.

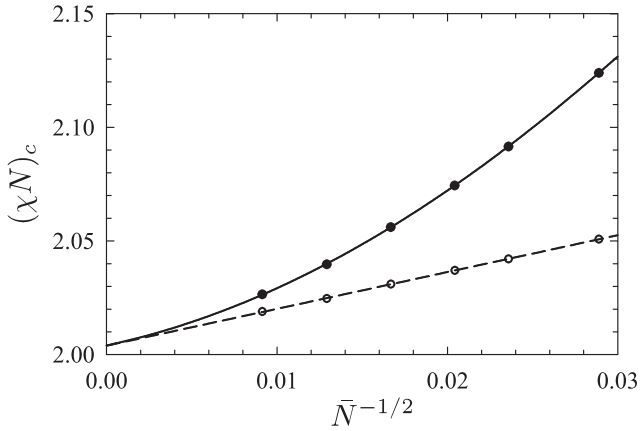

FIG. 8. Critical transitions from Table II plotted in terms of the nonlinear $\chi = z_\infty\alpha + c_1\alpha^2 + c_2\alpha^3$ (solid symbols) and the linear approximation $\chi \approx z_\infty\alpha$ (open symbols); the symbol size corresponds to our 0.1% uncertainty. Both curves correspond to the fit in Eq. (15).

Figure 8 plots the critical points from Table II in terms of the nonlinear χ from Eq. (12) and the linear approximation $\chi \approx z_\infty\alpha$. The size of the symbols corresponds to our estimated inaccuracy in α_c. Within this level of uncertainty, the critical points can be fit to the dashed line,

$$z_\infty\alpha_c N = 2.004 + 1.62\bar{N}^{-1/2}, \tag{15}$$

plotted in Fig. 8. Combining Eqs. (9), (12), and (15) provides an equivalent fit for the nonlinear χ, which is plotted in Fig. 8 with a solid curve. As evident from the plots, the nonlinear terms in $\chi = z_\infty\alpha + c_1\alpha^2 + c_2\alpha^3$ do not affect the leading-order terms in Eq. (2). Thus, the first fitting parameter in Eq. (15) implies $(\chi N)_c \approx 2.004$ for infinitely long polymers, which agrees well with the mean-field prediction of 2. The second fitting parameter gives $c \approx 1.62$ for the universal coefficient in Eq. (2), which is reasonably consistent with the previous estimate of $c \approx 1.5$.[24]

VI. DISCUSSION

Our new lattice model has proven to be remarkably efficient. Metastability effects were very small, even at the first-order ODT of the diblock copolymer melts, as evident by the near equivalence of the parallel-tempering runs from completely different states (see Fig. 4). Furthermore, the cumulants from the homopolymer blends exhibited precise fixed points (see Fig. 6) and accurate scaling (see Fig. 7), even for long polymers and large simulation boxes. The efficiency can be attributed to the low computational cost of performing the Monte Carlo steps (MCS), in part due to the zero-range interactions. The simplicity and high acceptance rate of the double-bridging move is another important contributing factor to the fast MC dynamics. Thanks to universality, the unphysical nature of the lattice is inconsequential.

The most significant property of the new model is its inherently large invariant polymerization index, $\bar{N}$. For our current choice

Published under license by AIP Publishing

of $Z = 5$, $\bar{N} = 59.9N$, whereas for the $Z = 1$ version of the model, it is only $\bar{N} = 4.51N$.[11] Hence, for a given $\bar{N}$, the single occupancy model requires the chains to be $59.9/4.51 \approx 13$ times longer. Given that block exchange is the only way long chains can cross in the $Z = 1$ model, this could easily increase the computational cost by 2 or 3 orders of magnitude. Furthermore, the simulation box needs to contain $\sqrt{59.9/4.51} \approx 3.6$ times more monomers in order to simulate an equivalent volume of melt in terms of R_g, and the use of nearest-neighbor interactions will add another factor of about 2 to the cost. Thus, the multiple occupancy provides a tremendous computational advantage.

It is well understood that ordered block copolymer melts experience complicated finite-size effects due to incommensurability between their preferred dimensions and the size of the simulation box.[30] Naturally, this will reduce the stability of ordered phases, pushing the ODT to higher segregation. In the case of the lamellar phase, however, the morphology has considerable freedom to adjust its period by selecting different orientations.[26,31] For the boxes used in our simulations, the relative spacing between allowed periods is about 4%, which is fine enough to obtain a reasonably accurate free energy given its $(D - D_{eq})^2$ dependence near the equilibrium period, D_{eq}. Therefore, we believe that the slight differences in Fig. 5 between $(\chi N)_{ODT}$ and Eq. (1) and similarly between D and the SCFT prediction both represent real effects.

These differences in Fig. 5 increase smoothly as N decreases, and therefore, we attribute them to the gradual breakdown of universality, which cannot continue indefinitely. In fact, the polymeric behavior will be lost altogether once the polymerization becomes ridiculously small. The minimum N necessary for the universality will depend on the particular model or experimental system being considered. In the case of the current model, it appears that $N \gtrsim 30$ is required. This is somewhat more than the requirement for off-lattice models,[11–13] but that is a small price to pay for the increased efficiency of using a lattice.

If the universality does indeed require $N \gtrsim 30$, this would limit the simulations to $\bar{N} \gtrsim 2000$. Nevertheless, one could simply recalibrate the model with fewer monomers per site in order to handle smaller $\bar{N}$. Given that $\bar{N}$ is proportional to ρ_0^2, reducing the maximum occupancy from $Z = 5$ to $Z = 4$ should allow for $\bar{N} \approx 1000$ and $Z = 3$ could facilitate $\bar{N} \approx 600$. However, with a maximum of three monomers per site, the absence or presence of a vacancy may have an unduly large effect on the interaction energy. Even though it would reduce the efficiency of the simulation, it might be best to include nearest-neighbor interactions for $Z \leq 3$.

The fit in Eq. (15) was obtained by linear regression, which predicts 90% confidence intervals of 2.0040 ± 0.0004 and 1.62 ± 0.02 for the two fitting parameters. However, one needs to be cautious in accepting these estimated uncertainties, given the stringent assumptions behind linear regression. First, it assumes that the underlying relationship between α_c and $\bar{N}^{-1/2}$ is linear, which, of course, is only approximately true. Second, it assumes that the deviations from the linear relationship are caused by normally distributed random errors with a variance that is independent of $\bar{N}$, which is certainly not true. The situation for nonlinear fits (e.g., Fig. 1) is even more precarious, and so we do not attempt to estimate their uncertainties.

In the previous study by Beardsley and Matsen,[24] the extrapolation of $(\chi N)_c$ to infinite N was remarkably consistent with the mean-field prediction of 2. This evidence that the χ derived from diblock copolymer melts also works for homopolymer blends supports the belief that χ is independent of molecular architecture. Although our extrapolation of 2.004 in Fig. 8 only differs from the mean-field prediction by 0.2%, the deviation is nevertheless 10 times the uncertainty estimated by linear regression. This, however, can readily be attributed to the inaccuracy in z_∞, which violates the assumption of random errors. The inaccuracy in z_∞ originates from the two fits in Fig. 1, which are based on truncated Taylor series expansions [Eqs. (8) and (10)]. Although the statistical segment length, a, estimated from the first fit appears accurate, its value enters as a^{-3} in the second fit reducing the accuracy of z_∞. If we put our faith in the linear fit of Eq. (15), and instead determine z_∞ by requiring the extrapolation of $(\chi N)_c$ to match the mean-field value of 2, we obtain $z_\infty = 3.340$. Repeating the fit of $S(q^*)$ to ROL with this value gives $c_1 = 4.25$ and $c_2 = -8.94$. The resulting change in χ, however, is so small that it has no visible effect on the diblock copolymer ODTs in Fig. 5.

Our new estimate of $c = 1.62 \pm 0.02$ for the universal coefficient in Eq. (2) may seem to disagree with the previous estimate of $c \approx 1.5$, but this is likely due to a large inaccuracy in the latter value, which was obtained from a nonlinear fit. Extrapolation is notoriously unreliable, particularly when the data are nonlinear. This is why we chose to fit the open symbols rather than the solid symbols in Fig. 8. When we perform a 4-parameter polynomial fit to the solid symbols, we obtain $(\chi N)_c = 2.005 + 1.102\bar{N}^{-1/2} + 129\bar{N}^{-1} - 822\bar{N}^{-3/2}$, which closely matches the solid curve in Fig. 8. Despite the close match, the solid curve gives $c = 1.62$, whereas the 4-parameter fit gives $c = 1.10$. Extrapolation of the open symbols is far less ambiguous and thus much more trustworthy. The critical point data in Ref. 24 also exhibited a significant degree of curvature, and so the resulting prediction of $c \approx 1.5$ is prone to inaccuracy. In reality, the linearity of our results in Fig. 8 was remarkably fortuitous, which implies that it will be difficult to improve upon our estimate of c using alternative models.

VII. SUMMARY

Following the strategy of Wang,[20] we introduced a new model designed for efficient simulations of high-molecular-weight block copolymer melts, where monomers are restricted to the sites of an fcc lattice. Our current implementation is for $Z = 5$, where 80% of the sites contain 5 monomers and the remaining sites have 4 monomers. The multiple occupancy results in a high monomer density of $\rho_0 = 6.778/b^3$, which, in turn, leads to large invariant polymerization indices, $\bar{N}$. In addition to the usual advantages of a lattice model, the efficiency is further enhanced by limiting interactions to monomers within the same site. Despite the unphysical nature of the lattice, quantitative predictions are nevertheless possible on account of the universality of block copolymer phase behavior. This is achieved by mapping the parameters of the lattice model onto those of the standard Gaussian-chain model (GCM), using the Morse calibration.[8,11] The resulting relationship between the statistical segment length and the bond length of the lattice model is given by $a = 1.0447b$.

Published under license by AIP Publishing

The mapping between the Flory-Huggins χ parameter and the interaction parameter, α, of the lattice model is well approximated by $\chi \approx 3.346\alpha + 4.16\alpha^2 - 8.66\alpha^3$.

Our first application of the model examined the order-disorder transitions, $(\chi N)_{\mathrm{ODT}}$, of symmetric AB diblock copolymer melts. This was done by performing pairs of parallel-tempering simulations from ordered and disordered configurations. The simulations equilibrate relatively quickly, testifying to the efficiency of the Monte Carlo moves and providing consistent predictions for the ODTs. The resulting ODTs agreed well with the universal curve obtained from previous simulations [Eq. (1)]. There was, however, some deviation at small N, indicating that the model requires $N \gtrsim 30$ in order to exhibit universal behavior. Although this limits the simulations to $\bar{N} \gtrsim 2000$, lower values could be handled by recalibrating the model with fewer monomers per site.

Our second application examined the critical points, $(\chi N)_c$, of symmetric AB binary homopolymer blends. Accurate estimates of the transition were obtained using finite-size scaling. The resulting critical points, α_c, happened to follow a remarkably linear dependence on $N^{-1/2}$ over a wide range of polymerizations, $20 \leq N \leq 200$, allowing for a reliable extrapolation to infinite N. The limit was consistent with the mean-field prediction, $(\chi N)_c = 2$, to within 0.2%, supporting the notion that mean-field theory becomes exact in this limit and that the χ derived from AB diblock copolymers applies to all AB-type melts. Furthermore, the extrapolation predicted $c \approx 1.6$ for the universal coefficient in Eq. (2), which is reasonably consistent with the previous simulations in Ref. 24. We expect our new estimation to be the more accurate, given that it is based on a linear extrapolation between α_c and $N^{-1/2}$ [Eq. (15)].

Naturally, there are numerous other AB-type melts that this lattice model could be applied to. We are currently examining polydisperse diblock copolymer melts in order to determine the polydispersity corrections to Eq. (1). Given that monodisperse melts are experimentally impossible, it is essential to know these corrections in order to make quantitative predictions. Previous simulations for $\bar{N} \approx 200$ have already shown that even slight degrees of polydispersity can have a sizeable effect on the ODT.[14] The present model will allow us to extend that study to the entire range of experimentally relevant $\bar{N}$.

ACKNOWLEDGMENTS

This work was supported by NSERC of Canada, and computer resources were provided by SHARCNET of Compute Canada.

REFERENCES

[1] J. Glaser, J. Qin, P. Medapuram, M. Müller, and D. C. Morse, Soft Matter **8**, 11310 (2012).
[2] M. W. Matsen, J. Phys.: Condens. Matter **14**, R21 (2002).
[3] E. Helfand, J. Chem. Phys. **62**, 999 (1975).
[4] L. Leibler, Macromolecules **13**, 1602 (1980).
[5] A. N. Semenov, Sov. Phys. JETP **61**, 733 (1985).
[6] M. W. Matsen and F. S. Bates, Macromolecules **29**, 1091 (1996).
[7] G. H. Fredrickson and E. Helfand, J. Chem. Phys. **87**, 697 (1987).
[8] J. Glaser, P. Medapuram, and D. C. Morse, Macromolecules **47**, 851 (2014).
[9] P. Grzywacz, J. Qin, and D. C. Morse, Phys. Rev. E **76**, 061802 (2007).
[10] J. Qin, P. Grzywacs, and D. C. Morse, J. Chem. Phys. **135**, 084902 (2011).
[11] J. Glaser, P. Medapuram, T. M. Beardsley, M. W. Matsen, and D. C. Morse, Phys. Rev. Lett. **113**, 068302 (2014).
[12] P. Medapuram, J. Glaser, and D. C. Morse, Macromolecules **48**, 819 (2015).
[13] T. Ghasimakbar and D. C. Morse, Macromolecules **51**, 2335 (2018).
[14] T. M. Beardsley and M. W. Matsen, Phys. Rev. Lett. **117**, 217801 (2016).
[15] T. Pakula, Macromolecules **20**, 679 (1987).
[16] I. Carmesin and K. Kremer, Macromolecules **21**, 2819 (1988).
[17] H. Fried and K. Binder, J. Chem. Phys. **94**, 8349 (1991).
[18] T. Dotera and A. Hatano, J. Chem. Phys. **105**, 8413 (1996).
[19] O. N. Vassiliev and M. W. Matsen, J. Chem. Phys. **118**, 7700 (2003).
[20] Q. Wang, Soft Matter **5**, 4564 (2009).
[21] F. S. Bates, M. F. Schulz, A. K. Khandpur, S. Förster, J. H. Rosedale, K. Almdal, and K. Mortensen, Faraday Discuss. **98**, 7 (1994).
[22] R. Auhl, R. Everaers, G. S. Grest, K. Kramer, and S. J. Plimpton, J. Chem. Phys. **119**, 12718 (2003).
[23] J. Qin and D. C. Morse, J. Chem. Phys. **130**, 224902 (2009).
[24] T. M. Beardsley and M. W. Matsen, J. Chem. Phys. **147**, 044905 (2017).
[25] D. C. Morse and J. K. Chung, J. Chem. Phys. **130**, 224901 (2009).
[26] T. M. Beardsley and M. W. Matsen, Eur. Phys. J. E **32**, 255 (2010).
[27] K. Binder, Phys. Rev. Lett. **47**, 693 (1981).
[28] A. M. Ferrenberg and R. H. Swendsen, Phys. Rev. Lett. **61**, 2635 (1988).
[29] A. M. Ferrenberg and R. H. Swendsen, Phys. Rev. Lett. **63**, 1195 (1989).
[30] U. Micka and K. Binder, Macromol. Theory Simul. **4**, 419 (1995).
[31] A. Arora, D. C. Morse, F. S. Bates, and K. D. Dorfman, Soft Matter **11**, 4862 (2015).

Published under license by AIP Publishing